buildings

Article

A Comparative Study on the Distribution Models of Incident Solar Energy in Buildings with Glazing Facades

Shunyao Lu *, Xiaoqing Huang, Tao Chen and Zhengzhi Wang

School of Energy and Power Engineering, Nanjing Institute of Technology, Nanjing 211167, China; hxq-101@163.com (X.H.); chentaopipi@126.com (T.C.); wangzhengzhi@njit.edu.cn (Z.W.)
* Correspondence: lushunyao@njit.edu.cn

Abstract: The accurate distribution of solar energy on indoor walls is the basis of simulating the indoor thermal environment, and its specific distribution changes all the time due to the influence of solar azimuth and altitude angle. By analyzing the assumptions of each model, the existing solar energy distribution models are eight kinds in all and are divided into three categories. The solar radiation models in TRNSYS, EnergyPlus, and Airpak software all use the absorption-weighted area ratio method, which assumes that a single interior surface is a whole, but the detailed assumptions of the models used in the three software are different. In the Radiosity-irradiation method, the indoor surfaces are discretized into small surfaces for calculation. The calculation accuracy of solar radiation distribution indoors can be controlled by the number of discrete small surfaces. The Radiosity-irradiation method is implemented by using Matlab software programming in this paper. Through the numerical calculation and analysis of typical cases, the solar distribution results of the absorption-weighted area ratio method and the Radiosity-irradiation method all show the asymmetry. The asymmetrical ratio of direct solar radiation varies during the time between 7.96–9.89, and the minimum turns up at 11:30 in the summer solstice. The asymmetrical ratio of diffuse solar radiation is 3.23 constantly. The asymmetrical ratio of total solar energy is mainly influenced by the direct and diffuse solar feat gain and its value changes in the range from 3.4 to 4.45 in the summer solstice. Calculation comparison and error analysis on the solar radiation models used in TRNSYS, EnergyPlus, and Airpak software are conducted. There are significant errors in the simulation results of all three software. TRNSYS has the highest error among the three software as its results do not change over time. For EnergyPlus, the distribution ratio of floor 1 is too large. Airpak has the smallest error, but the solar radiation distribution ratios of the indoor surfaces near the south glazing facade are underrated, especially the indoor surfaces that have not been exposed to direct solar radiation.

Keywords: glazing facade; solar energy distribution; indoor thermal environment asymmetry; simulation software

Citation: Lu, S.; Huang, X.; Chen, T.; Wang, Z. A Comparative Study on the Distribution Models of Incident Solar Energy in Buildings with Glazing Facades. *Buildings* **2023**, *13*, 2659. https://doi.org/10.3390/buildings13102659

Academic Editor: Danny Hin Wa Li

Received: 17 September 2023
Revised: 13 October 2023
Accepted: 20 October 2023
Published: 22 October 2023

1. Introduction

High-rise buildings are the products of addressing issues such as increased population density and land scarcity in the development of urbanization and are also a symbol of urban economy and strength. As of 2022, 2071 buildings of 200 m and above and 211 super high-rise buildings of 300 m and above have been built worldwide [1]. Due to the large weight of high-rise buildings, glass curtain walls are often used for building envelopes because of structural safety considerations. Compared to walls, factors such as the transparency, weak insulation performance, and increased window-to-wall ratio of glass curtain walls significantly increase the solar radiation heat gain of buildings, which not only leads to an increase in building energy consumption but also exacerbates the deterioration of the indoor thermal environment. The near window area is prone to overheating [2], and the human body's thermal sensation under direct solar radiation is equivalent to an average radiation temperature increase of 11 °C [3]. Previous studies have shown that high-temperature environments have a significant impact on the thermal comfort [4], work efficiency [5], and physical health [6] of indoor occupants.

In the building thermal process, after transmitting through glass, solar radiation is absorbed by interior walls and increases wall temperature directly, and then indoor air temperature is increased by heat convection with interior surfaces. In glazing facade buildings, the increased solar heat gain leads to higher mean radiant temperature and air temperature. Beyond that, the asymmetrical distribution of solar heat gain intensifies indoor thermal environment asymmetry. Lots of research has been conducted on the thermal environment and energy consumption in conditions of different ratios of window to wall, windows' thermal properties, and shading devices [7–11]. These studies show that in glazing facade buildings, solar radiation's impact on the indoor thermal environment is much bigger than in traditional buildings. In fact, in buildings with glazing facades, the key to accurately simulating the indoor thermal environment is to grasp the accurate distribution of incoming solar energy on the indoor surfaces. The specific distribution of solar radiation heat indoors is constantly changing due to the influence of the sun's azimuth and altitude angles. For this issue, scholars have adopted different solar radiation distribution calculation models in the indoor thermal environment calculation process, and based on assumptions, these calculation models can be divided into three categories: (1) weight method, (2) Monte Carlo method, and (3) radiosity-irradiation method (RIM).

(1) Weight method

The first type of calculation model is relatively simple but has a large number. This type of model assumes that a single interior surface is a whole and the distribution of solar radiation on a single surface is uniform. Different models use different weights, and solar radiation is distributed on different internal surfaces based on wall weights.

Kraus [12] assumed that after passing through a transparent envelope, the direct solar radiation loses most of its directional character, so solar radiation distributes on each of the enclosure's surfaces uniformly after entering the room. Kontoleon [13,14] considered it a bit more complex, assuming that direct radiation enters the room through a window and maintains directionality. After the first reflection from the internal surface, it becomes diffuse radiation, which is uniformly distributed in the enclosure.

Cao [15] adopted the absorptance-weighted area ratios method, assuming that the incoming diffuse solar radiation and the reflected direct solar radiation are distributed within an enclosure. Software such as TRNSYS (version 18), EnergyPlus (version 23.2.0), and Airpak (version 3.0) have also applied this method, but there are some differences in their respective assumptions. The solar radiation model in TRNSYS [16] assumes that direct solar radiation loses directionality and becomes a part of scattered radiation after entering the room through the system. The solar radiation model in EnergyPlus [17] assumes that the incident direct solar radiation falls entirely on the ground, and some of it becomes diffuse radiation after being reflected by the ground. At the same time, the distribution rate on each wall can also be manually input. The solar radiation model in Airpak [18] assumes that the incident direct solar radiation maintains directionality after entering the room and lands on the indoor surfaces. Some of the direct radiation loses directionality after being reflected by the wall and becomes diffuse radiation. The specific comparative analysis will be conducted in the third section.

(2) Monte Carlo method

The Monte Carlo method is a probabilistic statistical method. It is more commonly applied to studies which require statistical analysis of data [19–21]. It is established based on the ray-trace method. Manni [22] used this method for solar distribution between buildings in the city.

(3) Radiosity-irradiation method (RIM)

The radiosity-irradiation method was proposed by Sparrow [23], which discretizes the indoor wall into N small walls when calculating indoor radiation heat transfer; Wen [24] developed a model that described the dynamic thermal behavior of a building based on the RIM algorithm.

In both the first and second methods, a single internal surface is considered as a whole, and the distribution ratio of solar radiation heat on each surface is given, which cannot reflect the asymmetry of solar distribution on a single surface. In the third type of method, the indoor surfaces are discretized into small surfaces for calculation. The calculation accuracy of solar radiation distribution indoors can be controlled by the number of discrete small surfaces, but its disadvantage is that it cannot be achieved through existing simulation software, and the calculation duration is long.

In this paper, the RIM algorithm will be programmed by using Matlab software (version R2019a) to calculate the accurate distribution of solar radiation in the enclosure, and the results will be compared and analyzed with the results calculated by the absorptance-weighted area ratios method. At the same time, error analysis will be conducted on the solar radiation distribution models in TRNSYS, EnergyPlus, and Airpak, which are commonly used software.

2. Radiation Models

2.1. Overview

A comparison is made between the absorptance-weighted area ratios method and the radiosity-irradiation method, which are widely used. On the one hand, the two algorithms both deal with direct solar radiation and diffuse solar radiation separately and figure out solar distribution in enclosures by weighted average calculation. On the other hand, these two algorithms are developed with different hypotheses. To highlight solar energy distribution's asymmetry, the floor, ceiling, east wall, and west wall are all divided into two equal surfaces. The surfaces in the zone near the glazing façade are marked as "1," and the surfaces in the adjacent zone are marked as "2". Therefore, the enclosure consists of ten surfaces, including the north wall and the south curtain wall, as shown in Figure 1. Some modifications are made to the two algorithms correspondingly.

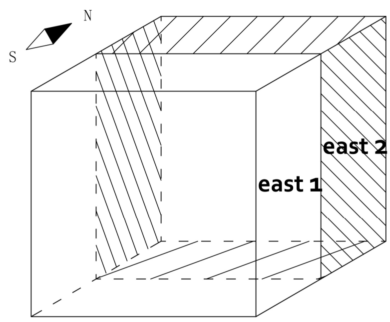

Figure 1. Divided surfaces within the enclosure.

This analysis focuses on the radiant exchange for the short wavelength solar radiation; long wavelength radiation is not included in this calculation.

2.2. Absorptance-Weighted Area Ratios Method

This algorithm is developed on these hypotheses: (1) each divided wall is considered as a single surface, and the absorbed solar radiation would be distributed over the whole surface uniformly; (2) all internal walls are treated as a Lambert surface, i.e., a perfect uniform and diffuse emitter, absorber and reflector of radiant energy, their parameters are the same except glazing surface; (3) incoming solar radiation cannot escape again.

Direct solar radiation distribution is calculated depending on sun patches and the beam spot formed on internal surfaces. A rectangular coordinates system is established on the plate of the floor. As shown in Figure 2, the beam spot on the floor plate is a parallelogram in south-oriented glazing facade buildings. It varies according to solar altitude and solar azimuth. For example, in Figure 2c, area 0463 is an irradiated area on floor 1, area 4576 is on floor 2, area 1578 is on the north wall, area 7896 is on east 2, and area 2369 is on east 1. All the cases shown in Figure 2 occur when solar azimuth is positive. If it is negative, the beam spot will arrive on the west wall.

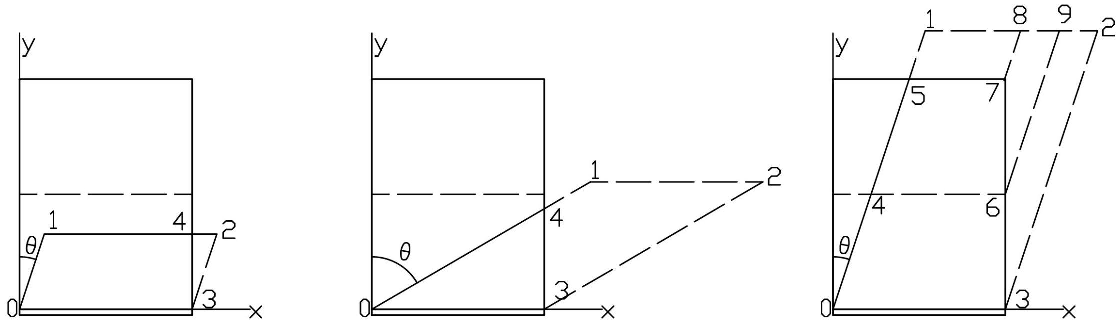

(**a**) (**b**) (**c**)

Figure 2. Beam spot on the plate of floor: (**a**) Low solar altitude and solar azimuth; (**b**) Medium solar altitude and large solar azimuth; (**c**) Large solar altitude and low solar azimuth.

u_i represents the proportion of the beam radiation hitting on surface i to the whole incoming direct radiation, $u_i = Q_i/Q = S_i/S$, where Q is the total incoming direct solar energy and Q_i is the direct solar radiation quantity that hits surface i. For example, in Figure 2a, u_1 of floor 1 is $S_{\square 0143}/S_{\square 0123}$, u_2 of east 1 is $S_{\triangle 234}/S_{\square 0123}$, and u_i of other surfaces is 0.

As shown in Figure 3, when direct solar radiation Q_i arrives at surface i, $(1-\rho)Q_i$ is absorbed by surface i and ρQ_i is reflected, where ρ is the reflectance of internal surfaces. An assumption is made that all the internal surfaces except surface i are considered as an ensemble, $(1-\rho)\rho Q_i$ is absorbed, and $\rho^2 Q_i$ is reflected by this ensemble. $\rho^2 Q_i$ arrives at surface i and the absorption and reflection are repeated until the end.

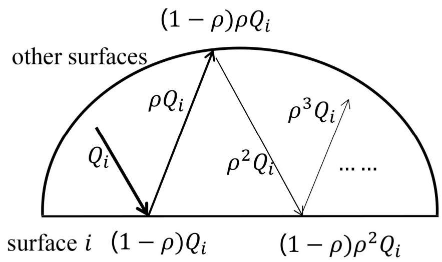

Figure 3. Absorbed and reflected radiation on surface i.

Absorbed by surface i from Q_i is:

$$\frac{Q_i}{1+\rho} = \frac{u_i}{1+\rho} Q, \tag{1}$$

Absorbed by other surfaces from Q_i is $\frac{\rho u_i}{1+\rho} Q$.

Absorbed by surface j from Q_i is $\frac{A_j}{A-A_i} \frac{\rho u_i}{1+\rho} Q$.

Absorbed by surface k from Q is $\frac{u_k}{1+\rho} Q + \sum\limits_{i=1, i\neq k}^{m} \frac{A_k}{A-A_i} \frac{\rho u_i}{1+\rho} Q$.

The direct solar radiation distribution parameter of surface k is:

$$p'_k = \frac{u_k}{1+\rho} + \sum_{i=1, i\neq k}^{m} \frac{A_k}{A-A_i} \frac{\rho u_i}{1+\rho}, \tag{2}$$

The distribution of the diffuse solar radiation can be calculated by the ratios of areas because of its non-directional character.

The diffuse solar radiation distribution parameter of surface k is:

$$p''_k = \frac{A_k}{A}, \tag{3}$$

The total direct radiation entering the enclosure is:

$$Q = S_{\square 0123} \sin(h) I_{dirN} \tau_{dir}, \tag{4}$$

where h is the solar altitude angle, I_{dirN} is the direct solar radiation intensity, and τ_{dir} is direct solar radiation's transmittance of glazing.

The total diffuse radiation entering the enclosure is:

$$Q' = f_g I_{dif} \tau_{dif}, \tag{5}$$

where f_g is the glazing area, I_{dif} is the diffuse solar radiation intensity, and τ_{dif} is diffuse solar radiation's transmittance of glazing.

The solar radiation absorbed by glazing is:

$$Q'' = S_{\square 0123} \sin(h) I_{dirN} \alpha_{dir} + f_g I_{dif} \alpha_{dif}, \tag{6}$$

where α_{dir} and α_{dif} is the direct and diffuse solar radiation absorptance of glazing. The absorbed solar energy is treated as the glazing's distribution part.

The total solar radiation distribution parameter of glazing is:

$$p_s = \frac{Q''}{Q + Q' + Q''} = \frac{S_{\square 0123} \sin(h) I_{dirN} \alpha_{dir} + f_g I_{dif} \alpha_{dif}}{S_{\square 0123} \sin(h) I_{dirN} (\tau_{dir} + \alpha_{dir}) + f_g I_{dif} (\tau_{dif} + \alpha_{dif})}, \tag{7}$$

The total solar radiation distribution parameter of the interior surface k is:

$$p_k = \frac{p'_k Q + p''_k Q'}{Q + Q' + Q''} = \frac{p'_k S_{\square 0123} \sin(h) I_{dirN} \tau_{dir} + p''_k f_g I_{dif} \tau_{dif}}{S_{\square 0123} \sin(h) I_{dirN} (\tau_{dir} + \alpha_{dir}) + f_g I_{dif} (\tau_{dif} + \alpha_{dif})}, \tag{8}$$

2.3. Radiosity-Irradiation Method

The absorbed solar energy for an interior wall is calculated using the RIM based on the view factor theory [12] and solves for the radiosity, irradiation, and absorbed radiant energy for a surface. Similar to the absorptance-weighted area ratios method, several assumptions are made: the direct solar radiation remains its directional character after being transmitted through the glazing; all surfaces are diffusely reflecting.

The irradiation for surface i is:

$$G_i = \sum_{j=1}^{N} F_{i-j} J_j, \tag{9}$$

where N represents the total number of divided surfaces, F_{i-j} is the view factor between surface i and surface j, and J_j is the radiosity for surface j.

The net radiation method is used for the analysis of indoor discrete interior surfaces. Figure 4 shows the radiosity schematic diagram of the internal surfaces and the interior surfaces of glazing.

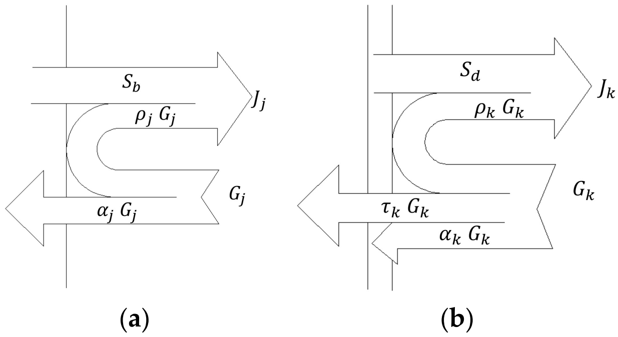

Figure 4. Radiosity for internal surface: (**a**) Internal surface *j*; (**b**) Interior surface *k* of glazing.

The radiosity for surface i is:

$$J_i = \rho_i S_{b,i} \cos\theta_i + S_{d,i} + \rho_i \sum_{j=1}^{N} F_{i-j} J_j, \tag{10}$$

where $S_{b,i}$ and $S_{d,i}$ are the solar beam and diffuse energy sources that have passed through the glazing, and θ_i is the direct solar radiation's incident angle for surface i. $S_{b,i}$ is non-zero only for surfaces that are irradiated directly by the solar beam energy and $S_{d,i}$ is non-zero only for the interior surfaces of the glazing.

Because Equation (9) is a linear algebraic equation, the solar radiosity J_i could be written as the sum of a solar beam radiosity $J_{b,i}$ and a solar diffuse radiosity $J_{d,i}$:

$$J_i = J_{b,i} + J_{d,i}, \tag{11}$$

The solar beam radiosity $J_{b,i}$ is:

$$J_{b,i} = C\rho_i S_{b,i} \cos\theta_i + \rho_i \sum_{j=1}^{N} F_{i-j} J_{b,j}, \tag{12}$$

where C is a judgment factor that represents whether surface i is irradiated or not. M judgment points are chosen on each surface by meshing. If m point is irradiated by a solar beam, the judgment factor is:

$$C = m/M, \tag{13}$$

The solar diffuse radiosity $J_{d,i}$ is:

$$J_{d,i} = S_{d,i} + \rho_i \sum_{j=1}^{N} F_{i-j} J_{d,j}, \tag{14}$$

The solar beam radiosity $J_{b,i}$ and the solar diffuse radiosity $J_{d,i}$ are calculated by solving the $N \times N$ equations.

The final absorbed solar flux for surface i is:

$$q_i = \alpha_i (S_{b,i} \cos\theta_i + G_i), \tag{15}$$

The absorbed solar energy for surface i is:

$$Q_i = q_i A_i, \tag{16}$$

Q_i represents the distribution part of solar energy for surface i.

The Radiosity-irradiation method is implemented by using Matlab software programming.

In Equation (12), the value of M is very important as it relates to calculation accuracy and calculation duration. The specific numerical determination process is as follows:

Due to the different solar altitude angles in different seasons, which can result in different exposure depths and transmittance of solar radiation, the independence test of discrete wall surfaces was conducted at 12:00 on the spring equinox, summer solstice, and winter solstice. Discretize the interior wall of a 3 m × 4 m × 3 m room for indoor solar radiation calculation. The corresponding number of discrete grids on the indoor wall surface is 66, 264, 1650, and 6600, with side lengths of 1 m, 0.5 m, 0.2 m, and 0.1 m, respectively. The calculation time is 2 s, 45 s, 8 min, 20 s, and 18 h, 33 min. As the number of discrete grids increases, the computational time increases exponentially.

Table 1 shows the calculation errors of solar radiation at 12:00 noon on three typical dates, namely the spring equinox, summer solstice, and winter solstice, under different discrete grid quantities.

Table 1. Discrete quantity, calculation duration, and calculation error.

Actual Solar Heat Gain W / Number of Discrete Grids and Calculation Duration	The Spring Equinox 3412.8		The Summer Solstice 1637.5		The Winter Solstice 3896	
	Solar Heat Gain Calculated W	Error $\Delta\varepsilon$	Solar Heat Gain Calculated W	Error $\Delta\varepsilon$	Solar Heat Gain Calculated W	Error $\Delta\varepsilon$
66 (2 s)	3060.5	10.3%	1000.4	38.9%	4363.9	−12%
264 (45 s)	3660.4	−7.3%	1743.5	−6.5%	3770.7	3.2%
1650 (8 m 20 s)	3376.4	1.1%	1501.5	8.3%	3906.9	−0.3%
3200 (18 h 33 m)	3374.4	1.1%	1727.6	−5.5%	3887.8	0.2%

As shown in Table 1, the larger the number of discrete grids on the surface, the smaller the calculation error and the longer the simulation time. Under the same computer hardware conditions, when the number of discrete grids reaches 6600, calculating the operating conditions at a single time can take up to 18 h and 33 min. Considering the calculation time and accuracy requirements, it is advisable to control the number of discrete grids within the range of 66 to 6600, and the corresponding edge length of the discrete element surface should be taken between 1 m and 0.1 m. For the vernal equinox and winter solstice with high incident solar radiation, the error is relatively small when the number of discrete grids is 1650 and 6600, but for the summer solstice, the calculation results of each discrete grid number have significant errors.

The reason for the calculation error is the error in determining the direct radiation source on the microelement surface. In the calculation model, whether the wall is illuminated is determined by whether the center point of the microelement surface is within the direct radiation irradiation spot. The judgment coefficient C is set to 1 or 0, but in reality, there is a situation where the discrete microelement surface is partially illuminated, and the judgment coefficient C is within the range of [0, 1]. Considering that the calculation accuracy should be ensured as much as possible while controlling the calculation time, 1650 discrete grids were selected in the calculation, with a single calculation time of 8 min and 20 s. At the same time, in order to improve computational accuracy, the direct radiation irradiation judgment points on individual discrete microelement surfaces were encrypted. Table 2 shows the error analysis of the number of judgment points on the microelement surface at 12:00 on the summer solstice when they were 4, 9, 16, and 25, respectively.

Table 2. Number of judgment points on discrete wall surfaces and calculation errors.

Actual Solar Heat Gain of the Summer Solstice W	Number of Judgment Points	Solar Heat Gain Calculated	Error $\Delta\varepsilon$
1637.5	4	1727.6	−5.5%
	9	1670.7	−2.0%
	16	1629.7	0.5%
	25	1629.9	0.5%

As shown in Table 2, the more judgment points lead to the higher the calculation accuracy. However, when the judgment points are encrypted to 16 judgment points, the calculation error is almost the same as the result of 25 judgment points. Therefore, while ensuring computational accuracy and effectively improving computational efficiency, 16 judgment points are taken on each discrete element surface, i.e., M = 16.

3. Results and Discussions

3.1. Room Description

The size of the room is L = 3 m, W = 4 m, H = 3 m. For the south-facing room located in Shanghai, the glazing is double-glass pane windows with low-E coating. The solar transmittance of the glazing is 0.6, the absorptance is 0.33, and the reflectance is 0.07. The internal surfaces of the room are assigned a solar absorptance of 0.6.

The distribution of solar energy at summer solstice is calculated using two methods. In RIM, the divided small surfaces' side length is 0.15 m. Therefore, the enclosure is divided into 1650 surfaces.

3.2. Distribution of Direct Solar Radiation

Before 9:00 and after 14:30, direct solar radiation cannot enter the south-facing room because of the solar azimuth. The distribution ratios for each surface from 9:00 to 14:30 are calculated, and the results are shown in Figure 5.

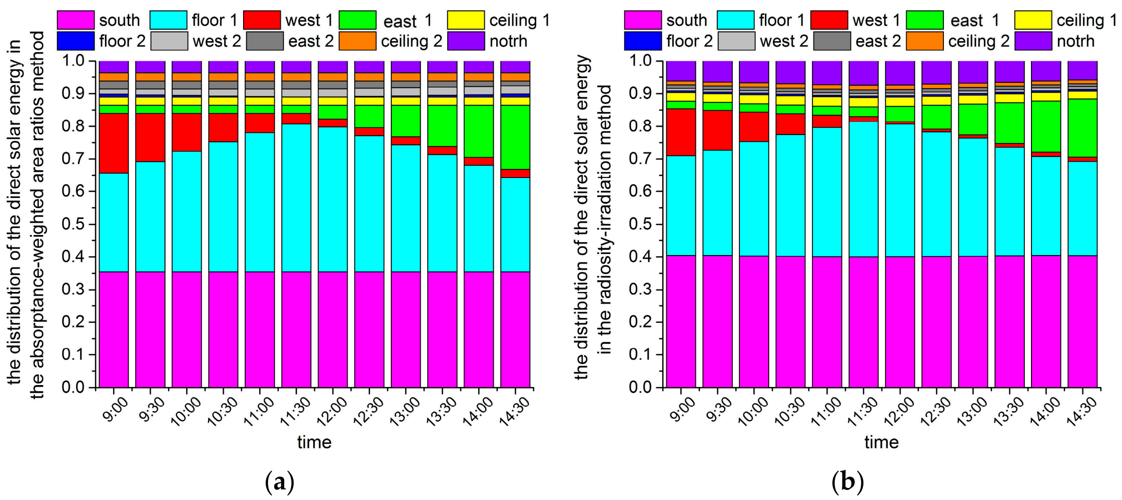

Figure 5. The distribution of the direct solar radiation: (**a**) Absorptance-weighted area ratios method; (**b**) Radiosity-irradiation method.

The variation trend of the surfaces' distribution ratio is similar in the two algorithms. There are some significant differences between the two calculation results. For instance, the ratio of south glazing is 35.5% constantly in the absorptance-weighted area ratios method but is around 40% in the RIM algorithm. The ratios of west 1 and east 1 in the absorptance-weighted area ratios method are slightly bigger than in RIM. The ratio of the north wall is 3.7% in the absorptance-weighted area ratios method and varies from 5.8% to 7.5% in the RIM algorithm. The differences occur because of the different assumptions of the two methods. In RIM, the south facade can receive the solar energy that is reflected from interior surfaces, so its ratio value is higher than in the absorptance-weighted area ratios method. The apex of floor 1 turns up at 11:30 because the solar azimuth (163°) is closer to 180 than at 12:00 (211°), and the floor 1 receives the most direct solar energy. Because the view factor between floor 1 and floor 2 is zero, floor 2 cannot receive the solar energy reflected by floor 1; therefore, the ratio of floor 2 is less than 0.5% at any time.

By dividing the sum of direct solar energy distributed in the zone near the glazing facade by the sum of energy in the adjacent zone, the asymmetrical ratio of the direct solar energy can be obtained. As shown in Figure 6, the asymmetrical ratio in the absorptance-weighted area ratios method is 8.04 constantly because the direct solar radiation cannot reach the adjacent zone during June 21st. In RIM, the asymmetrical ratio changes in the time period from 7.96 to 9.89, and the minimum appears at 11:30. The asymmetrical ratio, which is larger than 1 in both algorithms, shows the direct solar energy distribution in the zone mostly near the glazing facade.

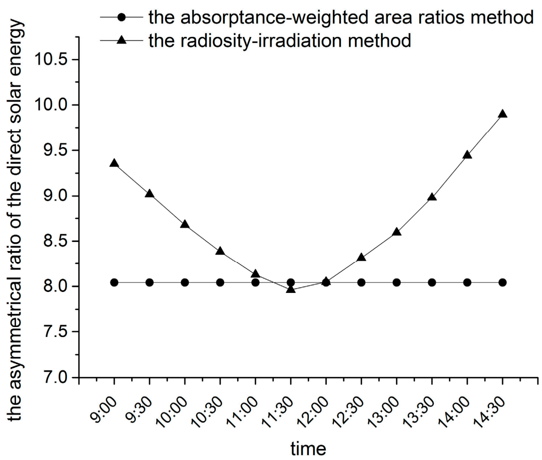

Figure 6. The asymmetrical ratio of the direct solar radiation distributed in the zone near the glazing facade to the adjacent zone.

3.3. Distribution of Diffuse Solar Radiation

The distribution of diffuse solar radiation is unaffected by the solar azimuth and altitude because it is non-directional. Therefore, the distribution ratio of diffuse solar radiation is constant, and its result in two algorithms is shown in Figure 7.

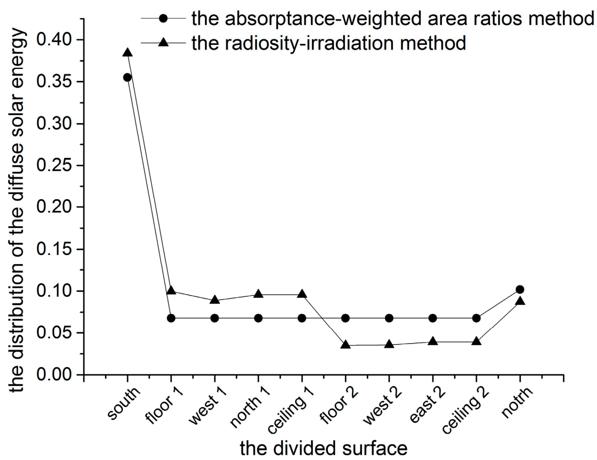

Figure 7. The distribution ratio of the diffuse solar radiation.

In the absorptance-weighted area ratios method, the distribution ratios of floor, ceiling, west and east walls are the same because the area and absorptance are the same. The distribution ratio of the north wall is higher because of its larger area. In RIM, the diffuse radiation transmitting through south-facing glazing is the radiation source, while the view factors between the glazing and surface 1 are larger than those between the glazing and surface 2. Therefore, the distribution ratios of surface 1 are larger than surface 2.

The asymmetrical ratio of diffuse solar energy distributed in the zone near the glazing façade to the adjacent zone in both algorithms is larger than 1. The result in RIM is 3.23, almost twice the result in the absorptance-weighted area ratios method, which is 1.68.

3.4. Distribution of Total Solar Radiation

The distribution of total solar radiation can be obtained by weighted calculation of direct and diffuse solar radiation. The results are shown in Figure 8.

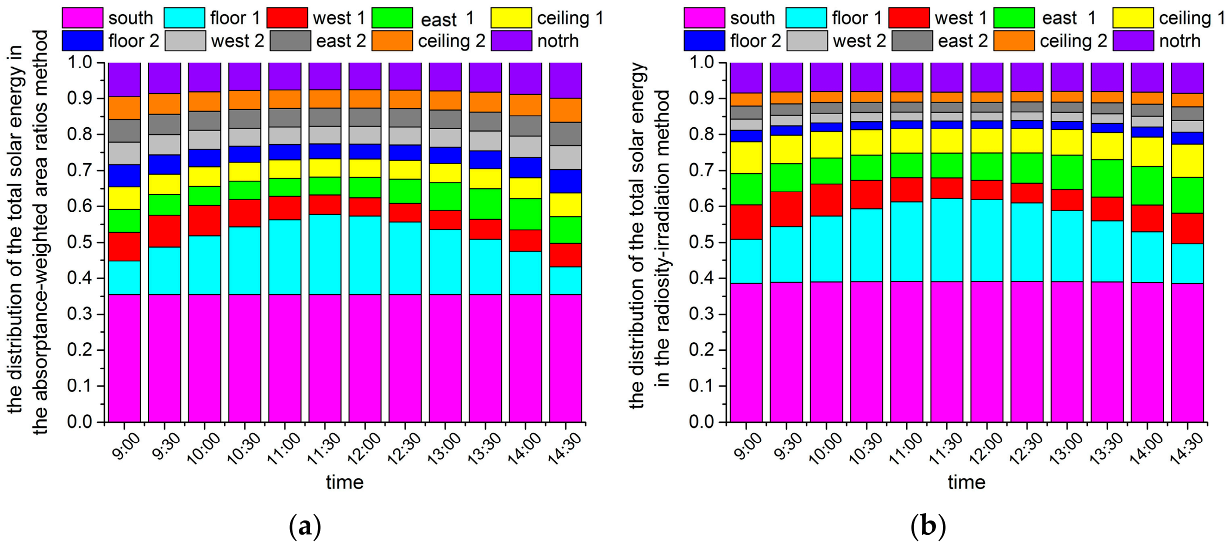

Figure 8. The distribution of total solar radiation: (**a**) Absorptance-weighted area ratios method; (**b**) Radiosity-irradiation method.

The distribution ratio of each surface varies with time in both algorithms, especially floor 1, west 1, and east 1. The difference in the south glazing's distribution ratio between the two algorithms is about 3%. In contrast to the direct solar energy, the distribution ratio of west 1 and east 1 in the absorptance-weighted area ratios method is slightly bigger than in RIM. The distribution ratio of surface 2 changes within the range of 5–6.6% in the absorptance-weighted area ratios method and changes from 2.2% to 3.7% in RIM.

There are obvious differences between the distribution ratio of total solar energy and direct solar energy. For instance, the distribution of total solar energy is more uniform than direct solar energy; the north wall's distribution ratio of total solar energy is almost the same in the two algorithms, while the north wall's distribution ratio of direct solar energy is quite different in the two algorithms. That is because, in the weighted calculation, the weight factors are the direct and diffuse solar heat gain of glazing facade buildings. As shown in Figure 9, for this south-facing room with the glazing facade, the diffuse solar heat gain is larger than the direct solar heat gain at any time on June 21st. Therefore, the total solar energy distribution is mainly influenced by the diffuse solar energy distribution.

Figure 10 shows the asymmetrical ratio of total solar energy distributed in the zone near the glazing façade to the adjacent zone. In the absorptance-weighted area ratios method, the asymmetrical ratio changes between 1.76–2.74. Its variation tendency is smooth because the distribution ratios of direct and diffuse solar energy are all constant. In RIM, the asymmetrical ratio changes between 3.4–4.45, the apex turns up at 12:30, and its value at 11:30 is smaller than at 11:00 and 12:00. That is because the minimum of the direct solar energy's asymmetrical ratio appears at 11:30 and the ratio between direct solar heat gain and diffuse solar heat gain reached its maximum at this time. The difference between the two algorithms is obvious and is around 1.7 at any time on June 21st.

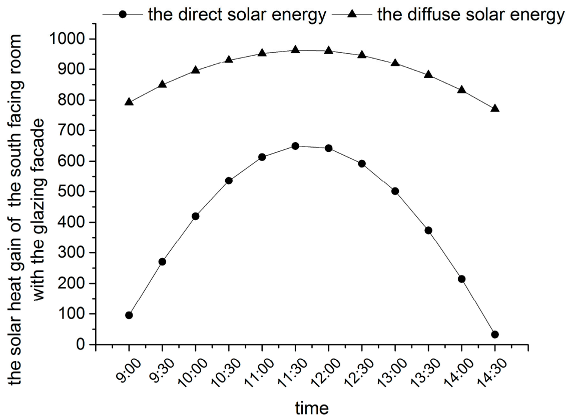

Figure 9. Solar heat gain of south-facing room with the glazing facade.

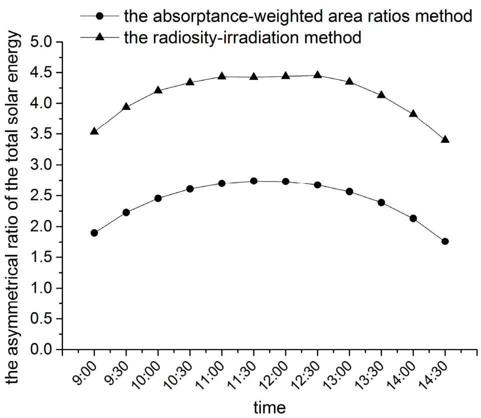

Figure 10. The asymmetrical ratio of the total solar energy distributed in the zone near the glazing facade to the adjacent zone.

3.5. Specific Distribution of Total Solar Energy in the Enclosure

In both two algorithms, the hypothesis is made that the solar energy absorbed by a single divided surface would be distributed over the whole surface uniformly. In the absorptance-weighted area ratios method, internal surfaces are divided into 10 small surfaces, while in RIM, the divided number is 1650. Therefore, the calculating result in RIM is more accurate and is presented in Table 3.

Table 3. Solar energy's distribution on each surface.

	South Glazing	**Floor**	**North Wall**	**Ceiling**	**West Wall**	**East Wall**
average W/m^2	68.4	49.3	21.3	18.7	15.9	18.6
maximum W/m^2	93.3	374.7	68.7	40.5	47.8	69.3

Results for solar energy on six internal surfaces at 12:00 on June 21st are shown in Figure 11. The contours have units of W/m^2; the contour interval is 50 W/m^2 for the floor and 10 W/m^2 for other surfaces.

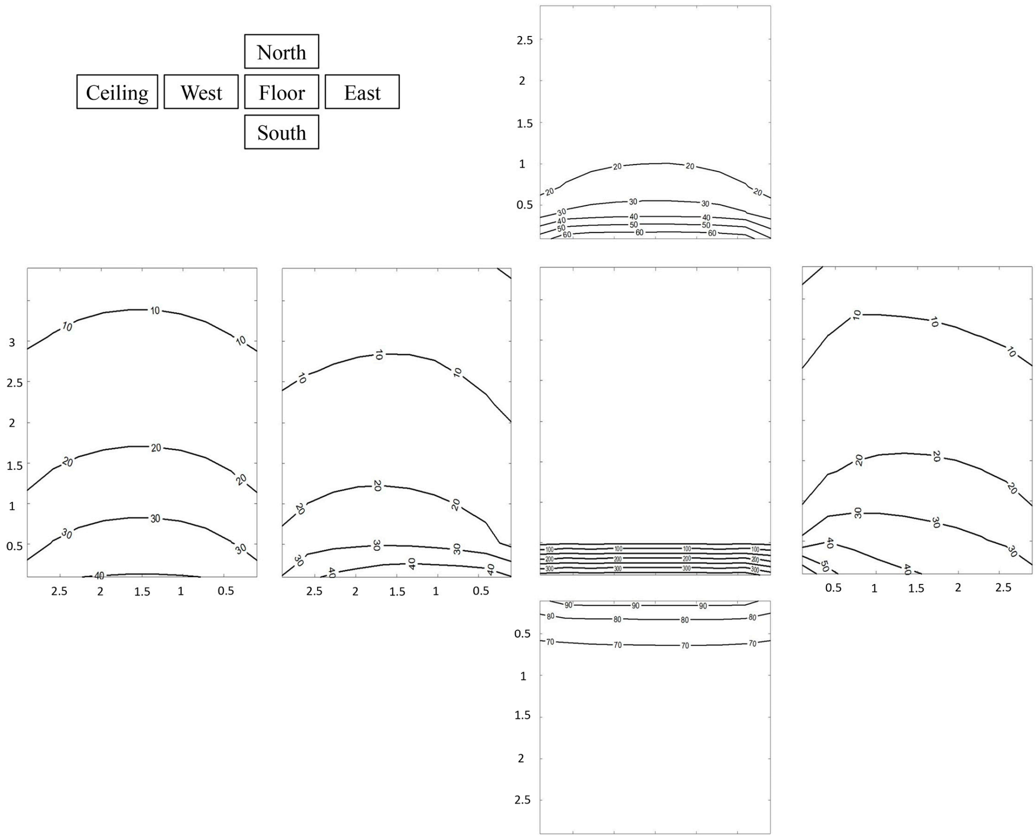

Figure 11. The distribution of total solar energy inside the enclosure.

The average solar heat gain of south glazing is the biggest among the six surfaces. That is because the south glazing absorbs a portion of incident solar radiation. On the floor, the area irradiated by direct solar energy receives a large amount of solar energy, and the maximum is 374 W/m^2 near the south glazing. On the north wall, the solar energy increases rapidly within the scope of 1 m near the floor. The solar energy distribution of the west wall and the ceiling is relatively uniform, but there are still visible differences between surfaces 1 and surfaces 2.

3.6. Error Analysis of Calculation Results of TRNSYS, EnergyPlus, and Airpak

The assumptions of indoor solar radiation distribution models in software such as TRNSYS, EnergyPlus, and Airpak are different, but the similarity is that all three software use the absorption-weighted area ratio method, which simulates a wall and cannot accurately express the actual distribution of solar radiation.

Calculation comparison and error analysis on the solar radiation models used in TRNSYS, EnergyPlus, and Airpak software were conducted. The standard value adopts the asymmetrical distribution model of solar radiation established in this paper, which can obtain the distribution intensity of solar radiation at any position on indoor surfaces. Two conditions on June 21st are calculated, 10:00 and 12:00, because the summer solstice is the day with the highest solar altitude angle throughout the year. The results of the distribution ratio of solar radiation on different indoor surfaces in different software are shown in Table 4.

Table 4. The distribution ratio of solar radiation on different indoor surfaces.

Time	Indoor Surface	Asymmetrical Distribution Model	TRNSYS	EnergyPlus	Airpak
June 21st 10:00	south	39.01%	38.40%	35.48%	35.48%
	floor 1	18.30%	9.99%	39.93%	16.39%
	west 1	8.95%	8.87%	3.14%	8.35%
	east 1	7.22%	9.56%	3.14%	5.41%
	ceiling 1	7.30%	9.56%	3.14%	5.41%
	floor2	2.51%	3.51%	1.06%	4.79%
	west 2	2.62%	3.55%	3.14%	5.24%
	east 2	2.97%	3.91%	3.14%	5.41%
	ceiling 2	3.03%	3.91%	3.14%	5.41%
	north	8.08%	8.74%	4.71%	8.11%
June 21st 12:00	south	39.09%	38.40%	35.48%	35.48%
	floor 1	22.73%	9.99%	39.70%	21.82%
	west 1	5.49%	8.87%	3.16%	5.06%
	east 1	7.54%	9.56%	3.16%	5.76%
	ceiling 1	6.76%	9.56%	3.16%	5.06%
	floor2	2.25%	3.51%	1.10%	4.11%
	west 2	2.40%	3.55%	3.16%	5.06%
	east 2	2.72%	3.91%	3.16%	5.02%
	ceiling 2	2.85%	3.91%	3.16%	5.06%
	north	8.17%	8.74%	4.74%	7.58%

As shown in Table 4, based on the comparison between the calculation results of three commonly used software and the calculation results of the asymmetrical solar radiation distribution model, the following analysis can be obtained:

(1) The calculation results of the solar radiation distribution model used in TRNSYS do not change over time and have significant errors. The distribution ratio of floor 1 is relatively small, while the distribution proportion of the other indoor surfaces is relatively large.

(2) The calculation results of the solar radiation distribution model used in EnergyPlus have significant errors too, as the distribution ratio of floor 1 is too large, and the distribution ratios of the other surfaces are relatively small. This is because it is assumed that all direct solar radiation falls to the ground after entering the room. The calculation results vary over time, and due to the constant distribution ratio of direct and diffuse solar radiation on each surface in the same room, the distribution of solar radiation on each surface is affected by the direct solar heat gain and the diffuse radiation heat gain.

(3) The calculation results of the solar radiation distribution model used in Airpak are relatively close to the calculation results of the asymmetrical solar radiation distribution model. The main error is the solar radiation distribution ratios of the indoor surfaces near the south glazing facade are underrated, especially the indoor surfaces that have not been exposed to direct solar radiation. For example, the east 1 and ceiling 1 at 10:00 on June 21st.

In summary, TRNSYS has the highest error among the three software, followed by EnergyPlus and Airpak.

4. Conclusions

The distribution of solar radiation within an enclosure was calculated with the use of the absorptance-weighted area ratios method and the radiosity-irradiation method algorithm. The calculated result in RIM is more accurate, and the asymmetrical ratio's difference between the two algorithms is around 1.7 at any time on June 21st.

The distribution of incoming solar radiation is asymmetrical. The distribution of direct solar radiation is mainly influenced by the beam spot formed on internal surfaces.

The asymmetrical ratio of direct solar radiation varies during the time between 7.96–9.89, and the minimum turns up at 11:30 in the summer solstice. The asymmetrical ratio of diffuse solar radiation is 3.23 constantly. For a south-facing room with a glazing façade, the direct solar heat gain is smaller than the diffuse solar heat gain during the summer solstice. Therefore, the asymmetrical ratio of total solar radiation is mainly influenced by the distribution of diffuse solar radiation, and its value changes in the range from 3.4 to 4.45.

There are some rules for solar energy distribution. For instance, the surfaces near the glazing receive higher solar energy, and for vertical walls, the surfaces near the floor receive higher solar energy because the direct solar radiation is more likely to hit the floor.

The asymmetrical distribution model of solar radiation established in this paper can obtain the distribution intensity of solar radiation at any position on indoor surfaces. This model is implemented using Matlab software programming, and the distribution of solar radiation at any time in any building can be calculated.

The solar radiation models in TRNSYS, EnergyPlus, and Airpak software all use the absorption-weighted area ratio method, but the detailed assumptions of the models are different. All three software simulates a single surface as a whole and cannot accurately express the actual distribution of solar radiation. Calculation comparison and error analysis on the solar radiation models used in TRNSYS, EnergyPlus, and Airpak software are conducted. There are significant errors in the simulation results of all three software. TRNSYS has the highest error among the three software as its results do not change over time. For EnergyPlus, the distribution ratio of floor 1 is too large. Airpak has the smallest error, but the solar radiation distribution ratios of the indoor surfaces near the south glazing facade are underrated. Especially the indoor surfaces that have not been exposed to direct solar radiation.

Author Contributions: Conceptualization, S.L. and X.H.; methodology, S.L.; software, S.L. and X.H.; validation, T.C.; formal analysis, T.C. and Z.W.; investigation, T.C.; writing—original draft preparation, S.L. and Z.W.; writing—review and editing, S.L. and Z.W.; visualization, T.C.; funding acquisition, S.L. All authors have read and agreed to the published version of the manuscript.

Funding: This work was supported by the Scientific Research Foundation of Nanjing Institute of Technology (Grants No. YKJ201963).

Data Availability Statement: The data presented in this study are available on request from the corresponding author.

Conflicts of Interest: The authors declare no conflict of interest.

References

1. High-Rise Building Database. Council on Tall Buildings and Urban Habitat. Available online: https://www.ctbuh.org/ (accessed on 1 August 2023).
2. Bessoudo, M.; Tzempeliko, A.; Athienitis, A.K.; Zemreanu, R. Indoor thermal environmental conditions near glazed façade with shading devices- Part I: Experiments and building thermal model. *Build. Environ.* **2010**, *45*, 2506–2516. [CrossRef]
3. Arens, E.; Gonzalez, R.; Berglund, L. Thermal comfort under an extended range of environmental conditions. *ASHRAE Trans.* **1986**, *92*, 18–26.
4. He, B.J.; Wang, J.; Liu, H.; Ulpiani, G. Localized synergies between heat waves and urban heat islands: Implications on human thermal comfort and urban heat management. *Environ. Res.* **2020**, *193*, 110584. [CrossRef] [PubMed]
5. Sadeghi, M.; De Dear, R.; Morgan, G.; Santamouris, M.; Jalaludin, B. Development of a heat stress exposure metric–Impact of intensity and duration of exposure to heat on physiological thermal regulation. *Build. Environ.* **2021**, *200*, 107947. [CrossRef]
6. He, B.J.; Zhao, D.X.; Dong, X.; Zhao, Z.; Li, L.; Duo, L.; Li, J. Will individuals visit hospitals when suffering heat-related illnesses? Yes, but. . .. *Build. Environ.* **2021**, *208*, 108587. [CrossRef]
7. Feng, C.Q.; Ma, F.G.; Wang, R.; Xu, Z.; Zhang, L.; Zhao, M. An experimental study on the performance of new glass curtain wall system in different seasons. *Build. Environ.* **2022**, *219*, 109222. [CrossRef]
8. Hwang, R.L.; Shu, S.Y. Building envelope regulations on thermal comfort in glass facade buildings and energy-saving potential for PMV-based comfort control. *Build. Environ.* **2011**, *46*, 824–834. [CrossRef]
9. Xu, C.; Li, S.; Zhang, X. Application of the CPMV index to evaluating indoor thermal comfort in winter: Case study on an office building in Beijing. *Build. Environ.* **2019**, *162*, 106295. [CrossRef]

10. Hajdukiewicz, M.; Geron, M.; Keane, M.M. Calibrated CFD simulation to evaluate thermal comfort in a highly-glazed naturally ventilated room. *Build. Environ.* **2013**, *70*, 73–89. [CrossRef]
11. Singh, M.C.; Garg, S.N.; Jha, R. Different glazing systems and their impact on human thermal comfort—Indian scenario. *Build. Environ.* **2008**, *43*, 1596–1602. [CrossRef]
12. Kraus, R.; Winter, E.R.F.; Ibele, W. Investigation of the energy flows for transparent and nontransparent building façade. *Sol. Energy* **1993**, *51*, 481–493. [CrossRef]
13. Kontoleon, K.J. Dynamic thermal circuit modeling with distribution of internal solar radiation on varying façade orientations. *Energy Build.* **2012**, *47*, 139–150. [CrossRef]
14. Kontoleon, K.J. Glazing solar heat gain analysis and optimization at varying orientations and placements in aspect of distributed radiation at the internal surfaces. *Appl. Energy* **2015**, *144*, 152–164. [CrossRef]
15. Cao, S.W. *Room Thermal Process and Air-Conditioning Load*; Shanghai Scientific and Technological Literature Press: Shanghai, China, 1991; pp. 71–80. ISBN 7-80513-837-0. (In Chinese)
16. *TRNSYS*, version 18; A Transient System Simulation Program; Solar Energy Laboratory. University of Wisconsin-Madison: Madison, WI, USA, 2022.
17. *EnergyPlus*, version 23.2.0; Engineering reference–Version 23.2.0 Documentation; Ernest Orlando Lawrence Berkeley National Laboratory: Berkeley, CA, USA, 2023.
18. Fluent Inc. *Airpak 3.0 User's Guide*; Fluent Inc.: New York, NY, USA, 2007.
19. Oliveto, V.; Patel, B.N.; Park, K.; Smith, D.E.; Hughes, M.D.; Borca-Tasciuc, D.-A. Theoretical investigation of asymmetric light interfaces for increasing optical efficiency of luminescent solar concentrators via integration of finite element simulation results with Monte Carlo ray tracing. *Renew. Energy* **2023**, *218*, 119314. [CrossRef]
20. Liu, C.Y.; Zheng, X.R.; Yang, H.B.; Tang, W.; Sang, G.; Cui, H. Techno-economic evaluation of energy storage systems for concentrated solar power plants using the Monte Carlo method. *Appl. Energy* **2013**, *352*, 121983. [CrossRef]
21. Ahmadpour, A.; Dejamkhooy, A.; Shayeghi, H. Optimization and modelling of linear Fresnel reflector solar concentrator using various methods based on Monte Carlo Ray–Trace. *Sol. Energy* **2022**, *245*, 67–79. [CrossRef]
22. Manni, M.; Bonamente, E.; Lobaccaro, G.; Goia, F.; Nicolini, A.; Bozonnet, E.; Rossi, F. Development and validation of a Monte Carlo-based numerical model for solar analyses in urban canyon configurations. *Build. Environ.* **2020**, *170*, 106638. [CrossRef]
23. Sparrow, E.M.; Cess, R.D. *Radiation Heat Transfer*; Hemisphere: Washington, DC, USA, 1978; ISBN 0-07-059910-6.
24. Wen, J.; Smith, T.F. Absorption of solar energy in a room. *Sol. Energy* **2002**, *7*, 283–297. [CrossRef]